Optically Controlled Solid-Density Transient Plasma Gratings

S. Monchocé,[1] S. Kahaly,[1] A. Leblanc,[1] L. Videau,[2] P. Combis,[2] F. Réau,[1] D. Garzella,[1] P. D'Oliveira,[1] Ph. Martin,[1] and F. Quéré[1,*]

[1]*Commissariat à l'Energie Atomique, Lasers, Interactions and Dynamics Laboratory, DSM/IRAMIS, CEN Saclay, 91191 Gif sur Yvette, France*

[2]*Commissariat à l'Energie Atomique, DAM, DIF 91297 Arpajon Cedex, France*

(Received 8 November 2013; published 11 April 2014)

A general approach for optically controlled spatial structuring of overdense plasmas generated at the surface of initially plain solid targets is presented. We demonstrate it experimentally by creating sinusoidal plasma gratings of adjustable spatial periodicity and depth, and study the interaction of these transient structures with an ultraintense laser pulse to establish their usability at relativistically high intensities. We then show how these gratings can be used as a "spatial ruler" to determine the source size of the high-order harmonic beams produced at the surface of an overdense plasma. These results open new directions both for the metrology of laser-plasma interactions and the emerging field of ultrahigh intensity plasmonics.

DOI: 10.1103/PhysRevLett.112.145008 PACS numbers: 52.65.Rr, 42.65.Ky, 52.27.Ny, 52.38.-r

The study of high-intensity laser-matter interactions using high-power femtosecond lasers is driven by two main motivations. One is understanding the fundamental physics behind these highly nonlinear interactions, and the other exploring their potential applications, as in laser-driven particle acceleration [1] and high order harmonic generation [2]. Most of these experiments require reaching the highest possible effective laser field amplitude on target and/or optimizing the coupling with the resulting plasma.

One way to achieve this is by utilizing spatial modulations at the surface of a solid target. Periodic structures can couple the laser field efficiently with collective excitation modes, called plasmons, potentially resulting in high light absorption [3,4]. Sharp spatial features can also lead to large local field enhancements, which can enhance hard-x-ray emission [3,5]. Both can favor acceleration of the plasma particles to high energies [6–8].

This new direction of research has so far been based on fairly complex target engineering, which does not allow structure control during the experiment. This also excludes materials or systems that cannot be shaped on the required scale before laser irradiation, such as the nanometric foils typically used for laser ion acceleration. In this context, the ability to generate *in situ* tunable plasma structures from initially plain solid targets made of any material would be a major step forward. This would extend the domain of plasmonics to high field science [9] and open new possibilities for experimental investigations on fast electron transport [10,11].

In this Letter, we present and demonstrate experimentally a new, simple, and flexible scheme to produce optically controllable structured plasmas from plain solid targets, for high-field physics experiments. As a first implementation of this scheme, we create transient sinusoidal "plasma gratings" from flat silica targets, which we probe by measuring the diffraction pattern of the high-order harmonic beam produced at their surface by an ultraintense laser pulse. Conversely, we show that this scheme provides a straightforward experimental means of retrieving the size of the harmonic source in the target plane—a quantity that is very challenging to measure by conventional optical methods.

All experiments described in this Letter have been performed on UHI100, the 800 nm, 25 fs-100 TW, high temporal contrast ($\geq 10^{12}$ using double plasma mirrors [12]) laser of CEA-IRAMIS. When a small part of this beam of adequate intensity (hereafter called a prepulse) is used to irradiate the surface of a solid target, it ionizes this target and initiates a plasma expansion. This leads to an exponential density profile [13], $n \propto \exp(-z/L(\tau))$ at the plasma-vacuum interface at a delay τ after the prepulse. The velocity $C_s = dL/d\tau$, of this expansion is expected to depend on the fluence F of the prepulse, and this dependence constitutes the starting point of our scheme. We measure this dependence for a polished silica target exposed to a single 25 fs laser pulse, by probing the subsequent plasma expansion through the phase shift it induces on a weak probe pulse, measured with time-resolved Fourier-domain interferometry [14] using the scheme described in Ref. [15].

Figure 1(a) shows the spatial profile of this phase shift across the prepulse focal spot, at four different delays τ after the prepulse. Plasma expansion velocity C_s at a given prepulse fluence F is obtained from the temporal evolution of this phase shift. Figure 1(b) depicts the measured variation of C_s with F. Beyond a threshold required to turn the target into a plasma, C_s shows a quasilinear dependence on the prepulse fluence [Fig. 1(b)]. Hydrodynamic simulations with the 1D code ESTHER [16], in conditions comparable to those of this experiment,

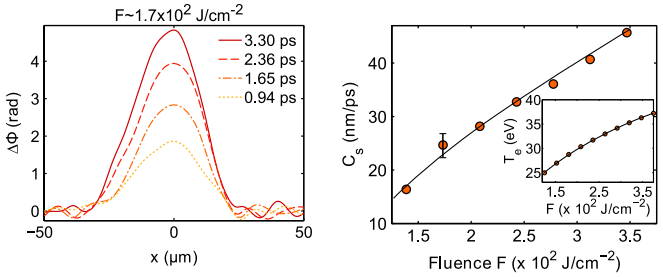

FIG. 1 (color online). (a) Temporal evolution of the spatially resolved phase shift induced on the Fourier-domain interferometry probe pulse by the plasma expansion triggered by a prepulse. (b) Fluence dependence of plasma expansion velocity C_s at the center of the prepulse beam, as deduced from the measured phase shifts. The inset plots T_e (at the critical plasma density n_c) as a function of prepulse fluence obtained from ESTHER simulations for a fused silica target under typical experimental conditions.

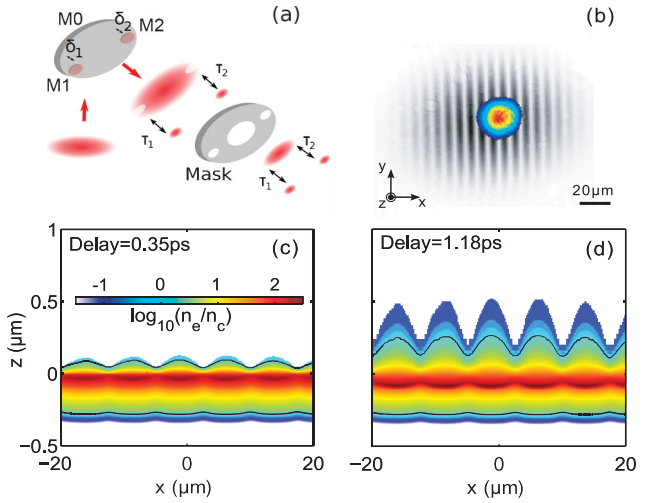

FIG. 2 (color). (a) Experimental scheme for the creation of optically controlled plasma gratings and their irradiation by an ultraintense pulse. (b) Resulting intensity distributions of the two interfering prepulse beams (gray scale) when they are perfectly synchronized ($\tau' = 0$), and of the main beam (colored scale) at focus. Panels (c) and (d) present the reconstructed plasma grating density calculated from ESTHER simulations at two different time delays τ. The black lines show the isodensity contours at $n = n_c$.

show that this variation can be predominantly attributed to an increase of the electron temperature T_e with the prepulse fluence [inset in Fig. 1(b)], due to the increase in absorbed laser energy.

Based on this result, a spatial structure can be induced at the surface of an initially flat solid target, prior to the arrival of a main ultraintense pulse, through the irradiation of this target by a spatially shaped prepulse beam [fluence $F(x) = F_0 f(x)$], at a variable delay τ before the main pulse. The dependence of C_s on F then leads to the progressive growth in time of a modulation on the surface of the overdense plasma. A simple way of achieving very fine spatial structures (potentially down to $\approx\lambda/2$, λ being the prepulse wavelength) with this approach, consists in using the spatial interferences of several beams to shape the prepulse fluence on target—a scheme then analogous to transient grating spectroscopy [17,18].

To demonstrate this idea, we create sinusoidal transient plasma gratings by interfering two synchronized prepulse beams on target. Experimentally, this is easily achieved by placing two 10 mm diameter mirrors on diametrically opposite edges of the UHI100 laser beam [$M1$ and $M2$ in Fig. 2(a)], just in front of one of the large mirrors [$M0$ in Fig. 2(a)] used for the main beam. Both beams are focused on a silica target by the same off axis parabolic mirror, and thus, cross at an angle on this target, where they interfere, producing a focal spot intensity pattern as shown in gray scale in Fig. 2(b). The fringe period λ_g is given by $\lambda_g = \lambda f/D_p$—with D_p the distance between the prepulse mirrors, and f the focal length of the focusing optics—and can be varied through any of these three parameters (Here, $D_p = 55$ mm, $f = 500$ mm, and $\lambda = 0.8$ μm leading to $\lambda_g = 7$ μm). The peak fluence of each individual prepulse on target is high enough ($\sim 1.7 \times 10^2$ J/cm^2) to create a dense plasma at the surface of silica.

We first carry out hydrodynamical simulations to study the plasma structure resulting from such an intensity distribution. For typical lateral scales λ_g in the μm range and expansion velocities of the order of 30 nm/ps, $L(\tau) = C_s\tau \ll \lambda_g$ for delays $\tau \leq 3$ ps used in the experiment, implying that 2D hydrodynamical effects can be neglected. Therefore to determine the time-dependent plasma electron density map $n_e(x, z, \tau)$ in this regime, we performed 1D ESTHER simulations, at different laser fluences F between 0 and F_0. This provides a collection of 1D density profiles at time τ, $n_e^{1D}(F, z, \tau)$, from which we deduce the 2D structure of the modulated plasma using $n_e(x, z, \tau) = n_e^{1D}(F_0 f(x), z, \tau)$.

The resulting density profiles $n_e(x, z, \tau)$ at two different delays are displayed in Figs. 2(c) and 2(d), while the complete temporal evolution $n_e(x, z, \tau)$ is provided in [19]. We observe that the fluence variation in the focal plane gives rise to periodic modulations of the critical density surface [solid black lines in Figs. 2(c) and 2(d)]. This solid density plasma grating retains the periodicity of the driving prepulse intensity modulation and expands in time, thus allowing for a control of grating periodicity and depth through the focusing configuration and delay time, respectively. The maximum modulation depth that can be achieved with these gratings is typically of the order of λ_g, beyond which two-dimensional hydrodynamical expansion effects are expected to significantly affect and smear out the spatial structure.

We now turn to the experimental demonstration of plasma gratings growth and control. A central portion of the UHI100 beam of adjustable diameter D is used to produce a main pulse that is focused on the target by the

same optics as the prepulses and interacts with the structured plasma they have created, thus acting as a high-intensity probe. The delay between the main pulse and the prepulses, $\tau = (\tau_1 + \tau_2)/2$ as well as the delay between the two prepulses, $\tau' = (\tau_1 - \tau_2)$ are adjustable. The prepulses are reflected from the back face of the small mirrors, so that the group delay accumulated in the glass substrate makes it possible to achieve $\tau = 0$ [15].

Figure 2(b) shows a superposition of the focal spot of the main pulse (color image) and of the interference pattern of the two prepulse beams on the target surface (gray image). The small diameter of the prepulse beams ensures that they each produce a much larger focal spot than the main beam, allowing it to interact with a uniform plasma grating. For diffraction-limited focusing, the number of grating periods N illuminated by this main pulse scales as D_p/D.

To visualize the existence of such a grating and to confirm that the structure survives when exposed to high intensities, we study high order harmonic generation (HHG) occurring when the p-polarized main pulse interacts with this grating at oblique incidence (55°). HHG can occur through two now well-identified mechanisms, coherent wake emission (CWE) [20] and the relativistic oscillating mirror (ROM) [21] process, the relative weight of which depends on the interaction conditions [15,22]. Intuitively, one expects that HHG occurring on a plasma grating would result in a diffraction pattern on the harmonic beam in far field, which, due to the short wavelengths of these harmonics, constitutes a very sensitive probe of this grating. We measure this diffraction pattern for each individual harmonic using a flat field XUV grating spectrometer described in [15], the slit of which is oriented in the plane of the two interfering prepulse beams.

We perform the first set of experiments on CWE harmonics, which are typically generated at moderate intensities ($\sim 10^{16}$ W cm^{-2}) and for sharp plasmas [2,15], allowing us to test the grating under these conditions. In Fig. 3(a), we present the angularly resolved harmonic spectrum after diffraction from such a plasma grating with a main pulse intensity, $I = 2 \times 10^{16}$ W/cm^2, a prepulse delay of $\tau = 0.35$ ps and $\tau' = 0$ [as in Fig. 2(c)]. Experimentally, this is achieved by using a rather small diaphragm ($D = 2$ cm) to produce the main pulse, leading to a $N \approx 5$ grating periods within its focal spot.

As the delay τ' between the two prepulses increases, the diffraction pattern progressively vanishes and is no longer observed when it exceeds the pulse coherence time τ_c [Fig. 3(b)], i.e., when the two prepulses no longer interfere. The complete evolution as a function of τ' is shown in [19]. This demonstrates that the observed diffraction pattern indeed results from the modulated plasma expansion triggered by the spatially interfering prepulse beams.

We now expose the grating to more drastic conditions by looking at ROM harmonics, which are generated at relativistic intensities and for longer density gradients L,

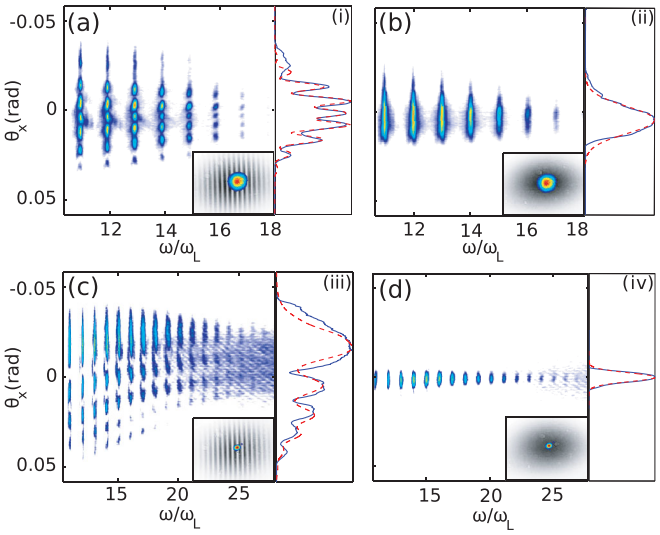

FIG. 3 (color). Panels (a) and (b) present experimental CWE angularly resolved harmonic spectra, respectively, at $\tau' = 0$ (maximum fringe contrast) and $\tau' > \tau_c$ (no grating) for short gradient ($\tau = 0.35$ ps) and $I_{\max} = 2 \times 10^{16}$ W/cm^2. Panels (c) and (d) present similar measurement for ROM harmonics, now for long gradient ($\tau = 1.18$ ps) and $I_{\max} = 1 \times 10^{18}$ W/cm^2. The blue lines in (i)–(iv), respectively, correspond to lineouts of the 12th harmonic in (a)– (d). The red dashed lines in (i) and (iii) present the best fits obtained from our model, and in (ii) and (iv), the Gaussian beams calculated in the far field in the absence of plasma grating, using the values of the parameters w_n and α_n deduced from these fits in (i) and (iii). The insets show the spatial pattern of the prepulses measured at focus (gray scale) superimposed with the focal spot of the main pulse (colored scale).

corresponding to larger delays τ. Compared to the previous results, this higher intensity is obtained by using a larger diaphragm for the main pulse, which also results in a smaller number of grating periods within its focal spot ($N \approx 2$). Figure 3(c) shows the frequency-resolved diffraction pattern of ROM harmonics at $I = 1 \times 10^{18}$ W/cm^2, from the plasma grating obtained with $\tau = 1.18$ ps and $\tau' = 0$. The small number of illuminated fringes is responsible for the asymmetry in this diffraction pattern. As shown in Fig. 3(d), where $\tau' > \tau_c$, the effect of the prepulses relative delay is the same as for the CWE case, confirming the origin of this diffraction pattern. This demonstrates clearly that the plasma gratings survive during the interaction with the main pulse, despite its ultrahigh intensity. This makes them very suitable for diverse high field applications, such as the coupling of ultraintense laser fields with surface plasmons [4] or, as we now show, the implementation of original measurement schemes of laser-plasma interactions.

We have so far used the harmonics beam as a probe of the plasma gratings. Conversely, these gratings can act as a probe of the harmonic source, to determine its spatial properties in the target plane,which are relevant both for development of new light sources and understanding the

underlying physics [23–25]. For harmonic orders $n \gg 1$, this field $h_n(x)$ is not readily accessible in usual experiments, due to the difficulty of making adequate optics for this spectral range. What can easily be measured is typically $|H_n(k)|^2$, with $H_n(k) = \mathrm{FT}(h_n(x))$. the harmonic field after propagation up to a detector (far field). Determining $h_n(x)$ from this measurement is then essentially a phase-retrieval problem, as it requires the knowledge of the phase of $H_n(k)$, to perform an inverse Fourier transform.

Diffracting this source on a grating of suitable periodicity provides a simple solution to this standard problem: by inducing a modulation of known periodicity on the harmonic source, the grating can be used as a "spatial ruler" and release the indeterminacy associated with intensity measurements in the far field. We assume that the grating acts as a small perturbation on the HHG process: then, the nth harmonic field in the target plane in the presence of the grating, $h_n^g(x)$, can be expressed as $h_n^g(x) = h_n(x)g(x)$, where the function $g(x)$ describes the periodic amplitude and phase modulation induced by the grating. The diffraction pattern of the harmonic beam in the far field is then given by $S_n(k) = |\mathrm{FT}(h_n^g(x))|^2 = |H_n(k) * G(k)|^2$, i.e., it is the convolution of the unperturbed harmonic beam in the far field, $H_n(k)$, and of the Fourier transform $G(k)$ of $g(x)$, which essentially consist of a few Bragg peaks spaced by $2\pi/\lambda_g$ (Fig. 4).

The effect of the grating is, thus, to generate spatially shifted replicas of $H_n(k)$ on the detector (Fig. 4). Two distinct regimes can then be identified, depending whether the spacing between these replicas is larger [Figs. 4(a) and 4(b)] or smaller than the width of the unperturbed harmonic beam $H_n(k)$ [Figs. 4(c)–4(d) and 4(e)–4(f)]. In the first, most common case, these replicas are well separated, and no additional information on $H_n(k)$ is obtained from the diffraction pattern. In the second case, in contrast, the spatially sheared replicas of $H_n(k)$ overlap and interfere, and the resulting interference pattern is determined by the phase of $H_n(k)$. In this regime, a measurement of this diffraction pattern thus provides information on the spatial phase of $H_n(k)$, that is otherwise missing to determine $h_n(x)$. This is the basic idea that led to the invention of the well-known technique of ptychography [26]. Plasma gratings are ideal to implement this method, since they can be tuned in both periodicity and depth to fulfill the conditions on which it relies.

The experimental data of Fig. 3 are precisely taken in this regime of overlapping replicas: in the case of CWE, this is due to the large divergence of the unperturbed harmonic beam resulting from the strong intensity dependence of the harmonic phase [as in Fig. 4(c)] [23], while in the case of ROM, this is because of the low number of fringes $N \approx 2$ contained in the main focal spot [as in Fig. 4(e)]. To extract the information from these measurements, we calculate the diffraction pattern of the harmonic beam by using the

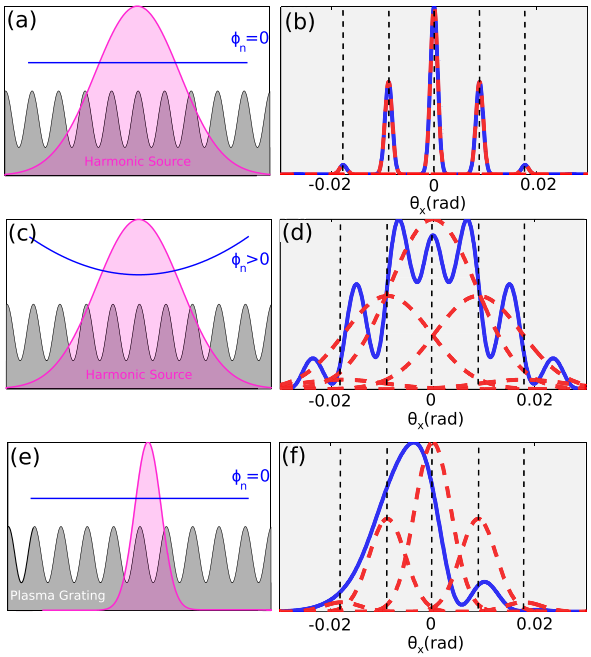

FIG. 4 (color online). Different regimes of diffraction from a grating. Panels (a)–(c)–(e) show different unperturbed source $[h_n(x)]$ amplitude (shaded red) and phase (blue) profiles, all modulated by the same sinusoidal grating (shaded gray). Panels (b)– (d)– (f) show the multiple replicas of the unperturbed beam $|H_n(k)|^2$ induced by the grating (dashed red) in the far field, which combination produce the total diffraction pattern (blue). In (a)–(b), the spacing between these replicas is larger than the divergence of the unperturbed beam, so that they do not overlap. In contrast, in (c)–(d) and (e)–(f), the replicas overlap and interfere, producing a pattern that depends on the spatial phase of $H_n(k)$.

previous formulas, assuming for $h_n(x)$ a Gaussian amplitude profile, with a source size w_n, and a parabolic phase profile $\Phi_n(x) = \alpha_n x^2$. We then use least square fitting method between this calculated pattern and the experimental data to determine the actual values of w_n and α_n.

The results of this fitting procedure in the CWE and ROM regimes are displayed in Figs. 3(i) and 3(ii), showing a remarkable agreement. Defining w_0 as the size of the focal spot of the main laser pulse, this leads to a source size of $w_{12} = (1 \pm 0.15)w_0$ for the 12th CWE harmonic, consistent with the low nonlinearity of CWE [2], and $w_{12} = (0.5 \pm 0.07)w_0$ for the 12th ROM harmonic, in excellent agreement with the predictions of particle-in-cell simulations [24,25]. The retrieved values of w_n and α_n are fully consistent with the divergences of the harmonic beams that we measure in the absence of plasma grating, as demonstrated by the plots in Figs. 3(ii) and 3(iv).

In conclusion, we have introduced a new scheme to generate and control modulated structures at the surface of solid density plasmas, demonstrated experimentally the generation of transient plasma gratings using this scheme, and shown that these structures survive relativistic

intensities. Diffraction patterns on harmonics produced from modulated plasma surfaces have been observed for the first time and exploited to perform the first determination of the harmonic source size in the target plane. In the future, more advanced measurement schemes can be implemented with plasma gratings, that would allow complete spatial characterisation of harmonic wave fields as well as their coherence properties, exploiting the latest developments in ptychographic algorithms [27].

More degrees of freedom can be easily introduced in this scheme, at the cost of only moderate additional complexity. The prepulse beam can, for instance, be frequency upconverted or focused with a shorter focal length optics, to achieve surface modulations with smaller spatial periods, potentially down to less than 1 μm. More complex surface plasma structures (e.g., nonsinusoidal or two-dimensional) can be induced by using more than two interfering beamlets. This scheme thus offers a great flexibility in terms of plasma structuring, opening numerous new possibilities in ultrahigh intensity plasmonics.

Insightful discussions with R. Marjoribanks are gratefully acknowledged. The research leading to these results has received funding from "Conseil Général de l'Essonne" though the ASTRE2010 Grant, of the Région île de France through SESAME, of the Triangle de la physique through PLASMOPT2, of OSEO through SAPHIR, of the European Research Council (ERC Grant Agreement No. 240013). The research leading to these results has received funding from LASERLAB-EUROPE (Grant Agreement No. 284464, EC's Seventh Framework Programme). S. Monchocé and S. Kahaly contributed equally to this work.

*fabien.quere@cea.fr

[1] A. Macchi, M. Borghesi, and M. Passoni, Rev. Mod. Phys. **85**, 751 (2013).
[2] C. Thaury and F. Quéré, J. Phys. B **43**, 213001 (2010).
[3] S. Kahaly, S. Yadav, W. Wang, S. Sengupta, Z. Sheng, A. Das, P. Kaw, and G. Kumar, Phys. Rev. Lett. **101**, 145001 (2008).
[4] T. Ceccotti *et al.*, Phys. Rev. Lett. **111**, 185001 (2013).
[5] G. Kulcsár, D. AlMawlawi, F. Budnik, P. Herman, M. Moskovits, L. Zhao, and R. Marjoribanks, Phys. Rev. Lett. **84**, 5149 (2000).
[6] D. Margarone *et al.*, Phys. Rev. Lett. **109**, 234801 (2012).
[7] H. Schwoerer, S. Pfotenhauer, O. Jäckel, K.-U. Amthor, B. Liesfeld, W. Ziegler, R. Sauerbrey, K. W. D. Ledingham, and T. Esirkepov, Nature (London) **439**, 445 (2006).
[8] A. Zigler *et al.*, Phys. Rev. Lett. **106**, 134801 (2011).
[9] A. P. Michael *et al.*, Nat. Photonics **7**, 796 (2013).
[10] H. Habara, K. Ohta, K. A. Tanaka, G. R. Kumar, M. Krishnamurthy, S. Kahaly, S. Mondal, M. K. Bhuyan, R. Rajeev, and J. Zheng, Phys. Rev. Lett. **104**, 055001 (2010).
[11] S. Kahaly, S. Mondal, G. R. Kumar, S. Sengupta, A. Das, and P. K. Kaw, Phys. Plasmas **16**, 043114 (2009).
[12] A. Lévy *et al.*, Opt. Lett. **32**, 310 (2007).
[13] Y. B. Zeldovich and Y. P. Raizer, *Physics of Shock Waves and High-Temperature Hydrodynamic Phenomena* (Dover Publications, New York, 2002).
[14] J. P. Geindre, P. Audebert, A. Rousse, F. Falliès, J. C. Gauthier, A. Mysyrowicz, A. D. Santos, G. Hamoniaux, and A. Antonetti, Opt. Lett. **19**, 1997 (1994).
[15] S. Kahaly, S. Monchocé, H. Vincenti, T. Dzelzainis, B. Dromey, M. Zepf, Ph. Martin, and F. Quéré, Phys. Rev. Lett. **110**, 175001 (2013).
[16] J. Colombier, P. Combis, A. Rosenfeld, I. Hertel, E. Audouard, and R. Stoian, Phys. Rev. B **74**, 224106 (2006).
[17] S. Mukamel, *Principles of Nonlinear Optical Spectroscopy* (Oxford University, New York, 1995).
[18] Y. Mairesse, D. Zeidler, N. Dudovich, M. Spanner, J. Levesque, D. Villeneuve, and P. Corkum, Phys. Rev. Lett. **100**, 143903 (2008).
[19] See Supplementary Material http://link.aps.org/supplemental/10.1103/PhysRevLett.112.145008 for movies showing the dynamics of the plasma grating simulated with ESTHER (Mov1), and the evolution of the experimental CWE diffraction pattern with τ' (Mov2).
[20] F. Quéré, C. Thaury, P. Monot, S. Dobosz, Ph. Martin, J.-P. Geindre, and P. Audebert, Phys. Rev. Lett. **96**, 125004 (2006).
[21] B. Dromey *et al.*, Nat. Phys. **2**, 456 (2006).
[22] A. Tarasevitch, K. Lobov, C. Wünsche, and D. von der Linde, Phys. Rev. Lett. **98**, 103902 (2007).
[23] F. Quéré, C. Thaury, J-P. Geindre, G. Bonnaud, P. Monot, and Ph. Martin, Phys. Rev. Lett. **100**, 095004 (2008).
[24] M. Yeung, B. Dromey, D. Adams, S. Cousens, R. Hörlein, Y. Nomura, G. Tsakiris, and M. Zepf, Phys. Rev. Lett. **110**, 165002 (2013).
[25] H. Vincenti, S. Monchocé, S. Kahaly, G. Bonnaud, Ph. Martin, and F. Quéré, Nat. Commun. **5**, 3403 (2014).
[26] Von W. Hoppe, Acta Crystallogr. Sect. A **A25**, 495 (1969).
[27] P. Thibault and A. Menzel, Nature (London) **494**, 68 (2013).